Evolution of energetic electron pitch angle distributions during storm time electron acceleration to megaelectronvolt energies

Richard B. Horne[1], Nigel P. Meredith,[2] Richard M. Thorne,[3] Daniel Heynderickx,[4] Roger H. A. Iles,[2] and Roger R. Anderson[5]

Received 7 November 2001; revised 28 March 2002; accepted 3 October 2002; published 14 January 2003.

[1] We investigate the pitch angle distributions of 0.15–1.58 MeV electrons observed during the 9–15 October 1990 storm measured by the Combined Release and Radiation Effects Satellite (CRRES) spacecraft. This storm period is characterized by an enhancement in the electron flux at $L \approx 4$ by more than an order of magnitude over the prestorm level. The overall change in flux at $L \approx 6.6$ is small in comparison. Previous work shows that radial diffusion underestimates the flux enhancement by up to a factor of 5 for $L \leq 4.5$ [*Brautigam and Albert*, 2000], indicating the need for an additional acceleration process. The pitch angle distributions presented here are examined for evidence of the acceleration mechanism. The distributions at $L \approx 2$ are rounded and are dominated by Coulomb collisions. They show little variation during the storm. The distributions at $L \approx 3$ are pancake-shaped before the storm, characteristic of pitch angle scattering by plasmaspheric hiss. During the main phase, they become broad and flat, and they evolve back into pancake distributions during the recovery phase. At $L \approx 4$–6, the pitch angle distributions are characterized as butterfly distributions at storm onset, and they become broad flat top distributions during the recovery phase. The flat top distributions persist throughout the ~3-day recovery phase and are observed in the region of highest flux enhancement. The flat top distributions are energy dependent and are broader at lower energies (30°–150°) than at higher energies (50°–130°). The higher energies exhibit a much faster fall off toward the loss cone than at lower energies. Inward radial diffusion should result in anisotropic distributions peaked near 90° and does not explain the observed energy dependence. Furthermore, the direction of diffusion is outward at higher energies. Model calculations of the pitch angles resonant with whistler mode waves show that flat top distributions are consistent with pitch angle and energy scattering in regions where $f_{pe}/f_{ce} \sim 1$. Although radial diffusion may be very important for particle energization, the observed pitch angle distributions provide strong evidence that wave particle interactions play an important role in the energization process. *INDEX TERMS:* 2720 Magnetospheric Physics: Energetic particles, trapped; 2788 Magnetospheric Physics: Storms and substorms; 2772 Magnetospheric Physics: Plasma waves and instabilities; 7867 Space Plasma Physics: Wave/particle interactions; *KEYWORDS:* pitch angle, magnetic storm, radiation belt, wave acceleration

Citation: Horne, R. B., N. P. Meredith, R. M. Thorne, D. Heynderickx, R. H. A. Iles, and R. R. Anderson, Evolution of energetic electron pitch angle distributions during storm time electron acceleration to megaelectronvolt energies, *J. Geophys. Res.*, *108*(A1), 1016, doi:10.1029/2001JA009165, 2003.

1. Introduction

[2] Enhancements in the relativistic electron flux at energies of a few MeV are frequently observed in the outer radiation belt. These enhancements are often associated with fast solar wind streams [*Baker et al.*, 1997; *Blake et al.*, 1997; *Li et al.*, 1997a; *Reeves*, 1998; *Iles et al.*, 2002] and coronal mass ejections [*Reeves et al.*, 1998a, 1998b; *Baker et al.*, 1998a, 1998b; *Buhler et al.*, 1997; *Li et al.*, 1998; *Selesnick and Blake*, 1998] impinging on the Earth's magnetosphere and which often drive geomagnetic storms. In one particular study covering more than a year of data, more than 90% of magnetic storms were found to be associated with relativistic electron flux enhancements at geostationary orbit [*Reeves*, 1998], although recent analysis suggests the figure is closer to 50% [*Reeves*, 2001]. Since ~MeV electrons are sufficiently energetic to penetrate the outer skin of spacecraft and cause internal charging, and since internal charging is responsible for anomalies on more

[1]British Antarctic Survey, Natural Environment Research Council, Cambridge, UK.
[2]Mullard Space Science Laboratory, University College London, Surrey, UK.
[3]Department of Atmospheric Sciences, University of California, Los Angeles, Los Angeles, California, USA.
[4]Belgian Institute for Space Aeronomy, Brussels, Belgium.
[5]Department of Physics and Astronomy, University of Iowa, Iowa City, Iowa, USA.

0148-0227/03/2001JA009165

than 20 satellites [*Wrenn and Smith*, 1996], flux enhancement events pose an important risk to satellites.

[3] Observations show that the flux enhancements must be due to electron acceleration processes within the Earth's magnetosphere [*Baker et al.*, 1989; *Li et al.*, 1997b]. Furthermore, since the relativistic electron flux is often enhanced above the prestorm level for many days after a magnetic storm, the acceleration process cannot be adiabatic. Several theories have been proposed that involve breaking one or more of the adiabatic invariants. They include inward radial diffusion driven by fluctuations in the large scale magnetospheric electric and magnetic fields, [*Schulz and Lanzerotti*, 1974], drift resonance with ULF waves [*Rostoker et al.*, 1998; *Liu et al.*, 1999; *Hudson et al.*, 2000; *Elkington et al.*, 1999], and Doppler shifted cyclotron resonance with whistler mode waves [*Li et al.*, 1997a; *Horne and Thorne*, 1998; *Summers et al.*, 1998; *Summers and Ma*, 2000]. Other theories, such as the recirculation theory [*Fujimoto and Nishida*, 1990], are essentially based upon a combination of radial diffusion and scattering by whistler mode waves. For more information on observations and theories see the recent reviews by *Li and Temerin* [2001], *Friedel et al.* [2002], and *Horne* [2002].

[4] Inward radial diffusion conserves the first two adiabatic invariants, but breaks the third. Provided the electron phase space density increases with radial distance (at constant adiabatic invariants), radial diffusion can result in substantial electron energization as the particles are transported across the magnetic field toward the Earth. Drift resonance with ULF waves also conserves the first two invariants and is essentially one of the drivers for radial diffusion. However, although radial diffusion can provide energization up to MeV energies, recent modeling of the 9 October 1990 storm showed that radial diffusion underestimates the high energy electron flux >500 MeV/G by more than a factor of 5 for $L < 4.5$ during the recovery phase of the storm [*Brautigam and Albert*, 2000]. Furthermore, during the recovery phase the radial profile of phase space density indicates a local maximum near $L = 4$, which is inconsistent with inward radial diffusion, and indicative of an additional local acceleration source. In a separate study, a local maximum near $L = 4$ was also found during the 3 November 1993 magnetic storm [*Miyoshi et al.*, 2001]. Spectral hardening of the electron flux was also found to increase first near the inner edge of the outer zone, and then to expand into the outer zone. Again this suggests a local acceleration source. A longer discussion of the evidence for and against radial diffusion and the importance of wave-particle interactions is given in the review by *Horne* [2002].

[5] Doppler shifted cyclotron resonance between electrons and whistler mode waves breaks the first, and hence all three invariants. The interaction results in electron loss from the radiation belts inside the plasmapause [e.g., *Lyons et al.*, 1972; *Thorne and Kennel*, 1971] and can energize the trapped part of the electron distribution up to MeV energies [*Summers et al.*, 1998; *Summers and Ma*, 2000]. The energization is more efficient in regions of low density, i.e., outside the plasmapause. Observations of whistler mode waves show that chorus amplitudes are enhanced during substorms [*Meredith et al.*, 2000] and that enhanced chorus amplitudes are associated with electron flux enhancements during storms that have substantial substorm activity [*Meredith et al.*, 2002a].

[6] Since Doppler shifted cyclotron resonance with whistler mode waves results in pitch angle scattering, it may be possible to distinguish among the acceleration processes by examining the electron pitch angle distribution during acceleration events. For example, assuming an isotropic source distribution pure radial diffusion in which the first two adiabatic invariants are conserved should result in distributions that are peaked near 90°. On the other hand, pitch angle scattering by whistler mode waves is energy-dependent and may only occur over a certain range of pitch angles, as determined by the wave properties and characteristic plasma frequencies.

[7] The purpose of this paper is to investigate the evolution of pitch angle distributions during storm time conditions to identify signatures of the electron acceleration mechanism. We consider the storm event of 9–15 October 1990, which was the subject of a detailed study on radial diffusion [*Brautigam and Albert*, 2000], allowing us to use their results as input to our study. The pitch angle data are discussed in relation to the two mechanisms of radial diffusion and pitch angle scattering.

2. Data Sources

[8] Satellite data used in this study were taken from the Combined Release and Radiation Effects Satellite (CRRES). The satellite was placed in an elliptical orbit with an apogee of 35,768 km, a perigee of 305 km, and an inclination of approximately 18°. The orbit period was approximately 10 hours. This satellite is one of the few that collected wave and particle data throughout the radiation belts. It is ideally suited to studying radial diffusion and wave particle interactions associated with radiation belt dynamics.

[9] High energy particle data in the range were obtained from the Medium Electron A (MEA) analyzer [*Vampola et al.*, 1992]. The MEA detector measures electron counts in seventeen energy channels and one background channel with central energies 0.153–1.58 MeV with a time resolution of 0.512 s. The instrument was fully calibrated and geometric factors for conversion from counts to fluxes have been determined. Background effects due to backscattered electrons and penetrating protons were monitored and subtracted from each channel during the data analysis. In the inner zone, the background correction is angle dependent because the tungsten collimator stops some protons which would otherwise be able to penetrate through the magnetic chamber walls and reach the background detector. The effect varies from −20% to +15% with respect to 90 degree incidence. The nominal background correction factors are correct only for 90 degree incident protons in this region. This is evident in the highest energy channels, where the true electron flux is very low. Proton contamination is not a significant problem in the outer radiation belt which is the focus of our attention here. The data was combined with magnetic field observations [*Singer et al.*, 1992] and carefully scrutinized to ensure the correct mapping to produce full pitch angle distributions.

[10] Low energy particle data in the range 0.112–18.7 keV were obtained from the Low Energy Particle Analyzer

(LEPA) [*Hardy et al.*, 1993] and wave data were obtained from the Plasma Wave Instrument (PWI) [*Anderson et al.*, 1992]. More details on the analysis of data from these two instruments is given by *Meredith et al.* [2000].

3. October 1990 Storm Period

[11] The case event studied here covers the storm period 9–15 October 1990, from now on referred to as the October 1990 storm period. The apogee of CRRES was in the dawn MLT sector at about 0400 MLT. Since freshly injected low energy electrons drift around the dawn sector and are a source of whistler mode waves, the dawn sector is a preferred region to capture both the particle signatures and the whistler mode waves that contribute to particle loss and acceleration.

[12] An overview of the event is shown in Figure 1. From top to bottom the figure shows, magnetic latitude, electron flux perpendicular to the magnetic field at 1.09 MeV, 214 keV, 14.3 keV, wave amplitude for lower band whistler mode chorus in the frequency range $0.1 < f/f_{ce} < 0.5$, solar wind speed (in red) and z component of the interplanetary magnetic field (IMF B_z, in black) from IMP 8, color coded Dst index, and AE index (line plot) with color coded K_p index. In each panel, one complete orbit consists of two vertical sweeps; the first corresponds to an outbound pass to apogee and the second corresponds to an inbound pass to perigee. The figure starts with an outbound pass (orbit 182 outbound). Note that there can be significant variation in the magnetic latitude from one complete orbit to the next, but the data are always within 30° of the magnetic equator. The vertical lines on the 8, 9, 10, 11, 12, and 13 October correspond to outbound orbits 182, 185, 186, 187, 189, 192, and 194 respectively, where more detailed data are presented below. The white line running along the top 5 panels shows the position of the plasmapause L_p calculated according to

$$L_p = 5.6 - 0.46K_p^* \quad (1)$$

where K_p^* is the maximum value of K_p in the previous 24 hours [*Carpenter and Anderson*, 1992].

[13] A magnetopause compression occurred on 9 October, corresponding to an increase in *Dst* and an increase in solar wind density (not shown). This was followed by a southward turning of IMF Bz and an increase in solar wind velocity that initiated a storm main phase on 10 October. The Dst index reached a minimum of −133 nT followed by a rapid recovery to about −50 nT and subsequently fluctuated around this level until 13 October, when it finally recovered. Therefore, the event can be considered as a strong storm ($-200 < Dst < -100$ nT) [*Loewe and Prölss*, 1997] followed by two or three moderate ($-100 < Dst < -50$ nT) and weak ($-50 < Dst < -30$ nT) storms.

[14] During the storm main phase, there was a significant reduction in the 1.09 MeV electron flux in the outer radiation belt ($L > 3.5$) followed by a recovery as the Dst index increased back to −50 nT. However, during the subsequent smaller storm intervals, where Dst fluctuated around −50 nT, the MeV flux continued to increase to values greater than the prestorm level. This suggests that the change in MeV electron flux cannot be due to an adiabatic effect alone. Some other processes must have been operating to increase the flux. During the first few hours of the main phase the flux at lower energies (214 keV) increased but by the time of minimum *Dst* there is a modest reduction compared to the prestorm level. The flux then increased above the prestorm level well before the increase in MeV flux. Furthermore, the slot region between the inner and outer radiation belts, which was clearly evident before the storm between $L \approx 2.5$–4, was filled in at energies of 214 keV during the onset of the recovery phase.

[15] In contrast to the MeV flux, the electron flux at 14.3 keV was significantly enhanced during the main phase. The enhancement occurred outside the plasmapause out to $L = 7$. During the subsequent recovery and period of weaker storms, the 14.3 keV flux showed significant variability, but remained elevated above the prestorm level. Lower band whistler mode chorus waves were also intensified outside the plasmapause, particularly during the storm main phase on 10 October, and during the recovery phase.

[16] Changes in the electron flux at selected intervals during the event can be seen more clearly in Figure 2. The orbits chosen correspond to the vertical colored lines in Figure 1. Only the outbound orbits are selected to provide a comparison at approximately the same MLT. Except for orbit 186, which corresponds to the drop out in the MeV electron flux, the orbits are chosen for equatorial crossings at low magnetic latitudes according to the Olsen-Pfitzer magnetic field model. No attempt has been made to correct the model for distortions in the magnetic field during the event. The data shown are for local pitch angle of 90°.

[17] The electron flux measurements at the two highest energy channels for $L < 2.5$ are known to be contaminated by energetic protons [*Johnstone et al.*, 1999], and are not considered here. The inner and outer radiation belt structure is clearly evident during the prestorm interval, orbit 182. The inner edge of the outer zone lies closer to the Earth for the higher energy particles. This is a characteristic signature resulting from the pitch angle scattering and loss of particles by plasmaspheric hiss [*Lyons et al.*, 1972].

[18] At the onset of storm main phase (orbit 185), structure in the radial flux profile appeared for $L \geq 5$ up to energies of at least 800 keV, and possibly higher. Structure appeared at lower L during the period of minimum Dst (orbit 186) and suggests multiple particle injection. This is consistent with the high level of substorm activity at this time, as measured by AE in Figure 1. By orbit 187 there is structure as low as $L = 2.5$, but outside $L = 3.5$ the radial flux profile is relatively smooth. In comparison to the main phase, the radial flux profile at all energies was relatively smooth during the recovery phase between orbits 187–194.

[19] The changes in the electron flux at a few hundred keV were very different to those >1 MeV. For $E > 1$ MeV, the flux in the outer zone dropped significantly during the main phase, first at large L (orbit 185) and then at all L (orbit 186). During the recovery phase (orbits 187–194), the MeV flux peaked near $L = 4.0$–4.5 and increased well above the prestorm level. By the end of the event (orbit 194), the MeV flux in the outer zone increased above the prestorm level for $3.5 \leq L \leq 6$. Conversely, the flux at a few hundred keV increased during the main phase at $L = 4$ but decreased for $L \geq 5$ (orbit 186) compared to the prestorm level. During the early recovery period (orbit 187), the flux

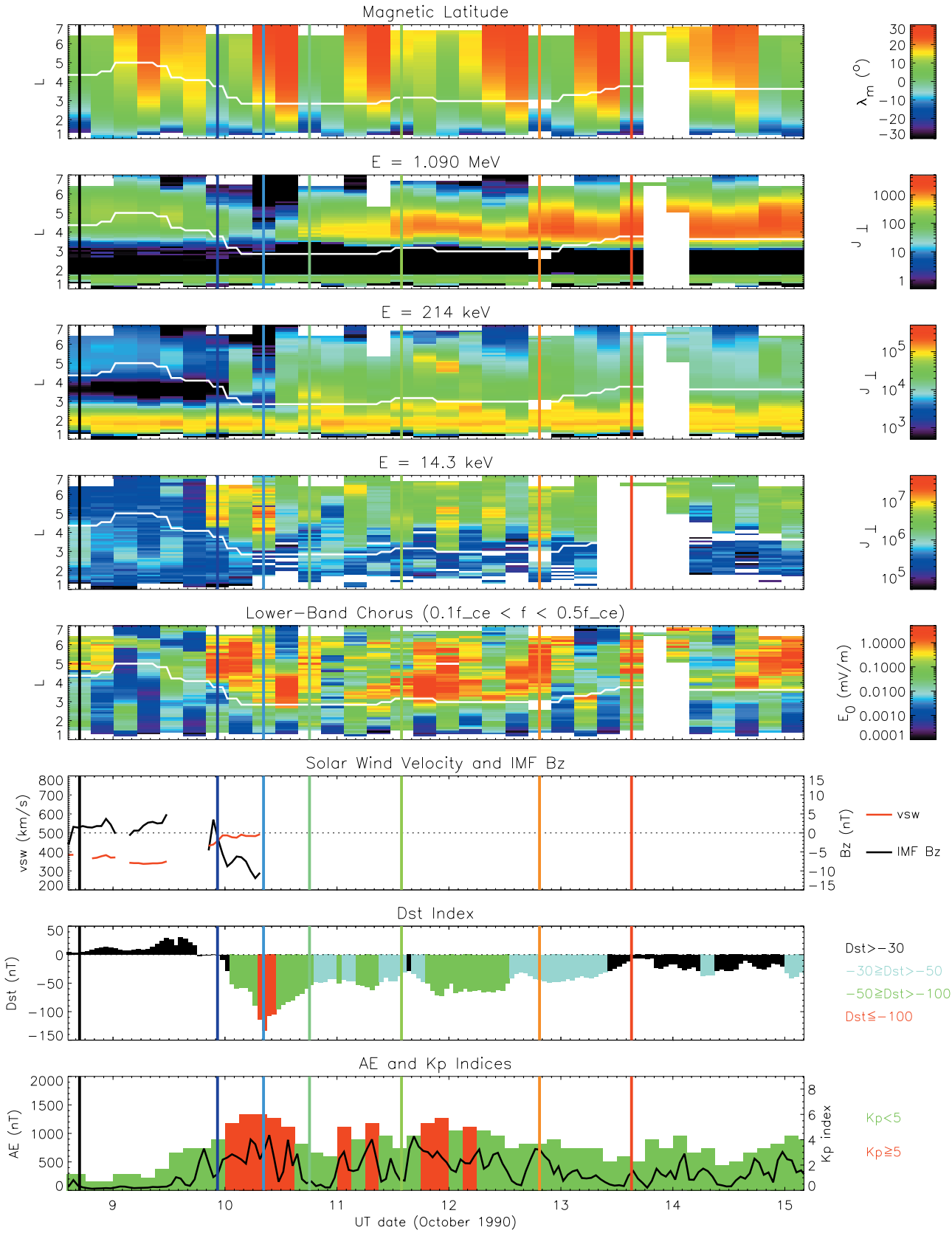
Magnetic Latitude
L
λm (°)
E = 1.090 MeV
J ⊥
E = 214 keV
J ⊥
E = 14.3 keV
J ⊥
Lower−Band Chorus (0.1f_ce < f < 0.5f_ce)
E0 (mV/m)
Solar Wind Velocity and IMF Bz
vsw (km/s)
Bz (nT)
vsw
IMF Bz
Dst Index
Dst (nT)
Dst>−30
−30≧Dst>−50
−50≧Dst>−100
Dst≦−100
AE and Kp Indices
AE (nT)
Kp index
Kp<5
Kp≧5
9
10
11
12
13
14
15
UT date (October 1990)

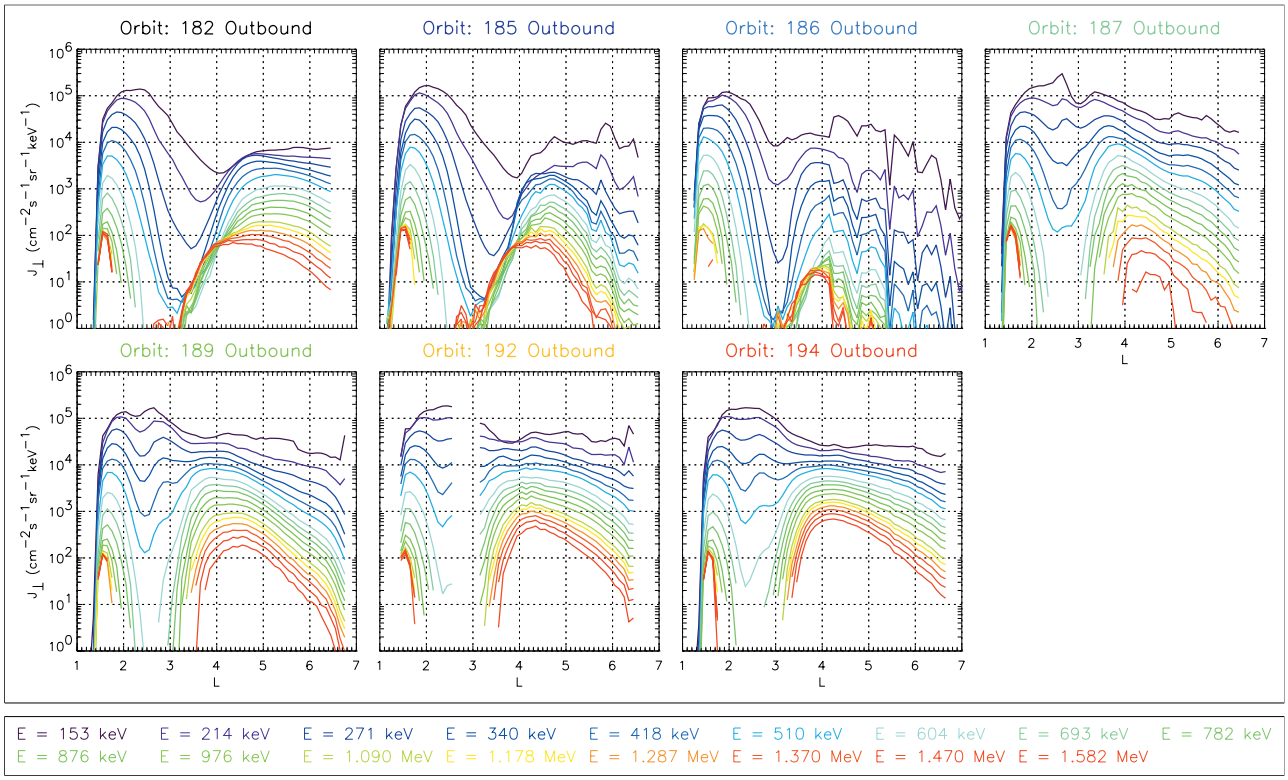

Figure 2. Electron flux at selected energies as a function of radial distance for the orbits indicated by the vertical bars in Figure 1. The data are for a local pitch angle of $\alpha = 90°$. The orbits are for prestorm (182), onset of main phase (185), minimum Dst (186), initial recovery (187), and recovery (189–194).

increased above prestorm levels at $L = 4$ and was comparable to prestorm levels for $L \geq 5$. During the rest of the recovery period the flux tended to decrease very slowly.

[20] The largest increase in ~1 MeV flux occurred near the inner edge of the outer zone, mainly between $L = 3–4$. For example, at 1 MeV the flux at $L = 4$ increased by an order of magnitude above the prestorm level by the end of the event. Conversely, for $L > 6$ there was very little change in the flux >1 MeV from prestorm levels. This illustrates the importance of measuring flux variations throughout the radiation belts and not relying on observations at geosynchronous orbit to infer changes at lower L.

4. Pitch Angle Distributions

[21] Pitch angle distributions for the October 1990 storm period are shown in Figure 3. The distributions are shown for the same outbound orbits as given in Figure 2 with increasing L running down the page. No pitch angle data are available for $L = 3$ on orbit 192 since the satellite was operating in a special mode to detect broad band VLF signals.

[22] The data shown are an average of the pitch angle distribution with a spatial resolution of 0.1 L. This provides much better count rate statistics at large L near apogee, but means that narrow features in the distribution are averaged out and that fast time variations are not captured. However, since the data presented above indicate that particle acceleration occurred over several days during the recovery phase, the gross features of the acceleration processes should still be present in the averaged pitch angle distributions.

[23] *Brautigam and Albert* [2000] used the Roederer L^* for their phase space density analysis. This enabled the drift shell to be identified. However, if we presented the pitch angle distributions as a function of L^* it would not result in a pitch angle distribution that is observable. Since we later wish to compare features in the distributions with resonant scattering by wave-particle interactions we present the observed pitch angle distributions in order to make this comparison.

[24] At $L = 2$ the pitch angle distributions appear rounded in the range $30° \leq \alpha \leq 150°$ at all the energies shown (153–782 keV) with a peak near 90°. The distribution at

Figure 1. (opposite) Data for the October 1990 storm period. The top five panels show data from the CRRES spacecraft; magnetic latitude, electron flux for a local pitch angle α of = 90° at 1.09 MeV, 214 keV, 14.3 keV, wave amplitude for lower band whistler mode chorus in the frequency range $0.1 < f/f_{ce} < 0.5$, solar wind speed (in red) and z component of the interplanetary magnetic field IMF B_z (in black) from IMP 8, color coded Dst index, and AE index (line plot) with color coded K_p index. The position of the plasmapause is marked on the upper 5 panels as a solid white line. The vertical lines are the outbound orbits 182, 185, 186, 187, 189, 192, and 194, selected for more detailed analysis of the flux and pitch angle distributions.

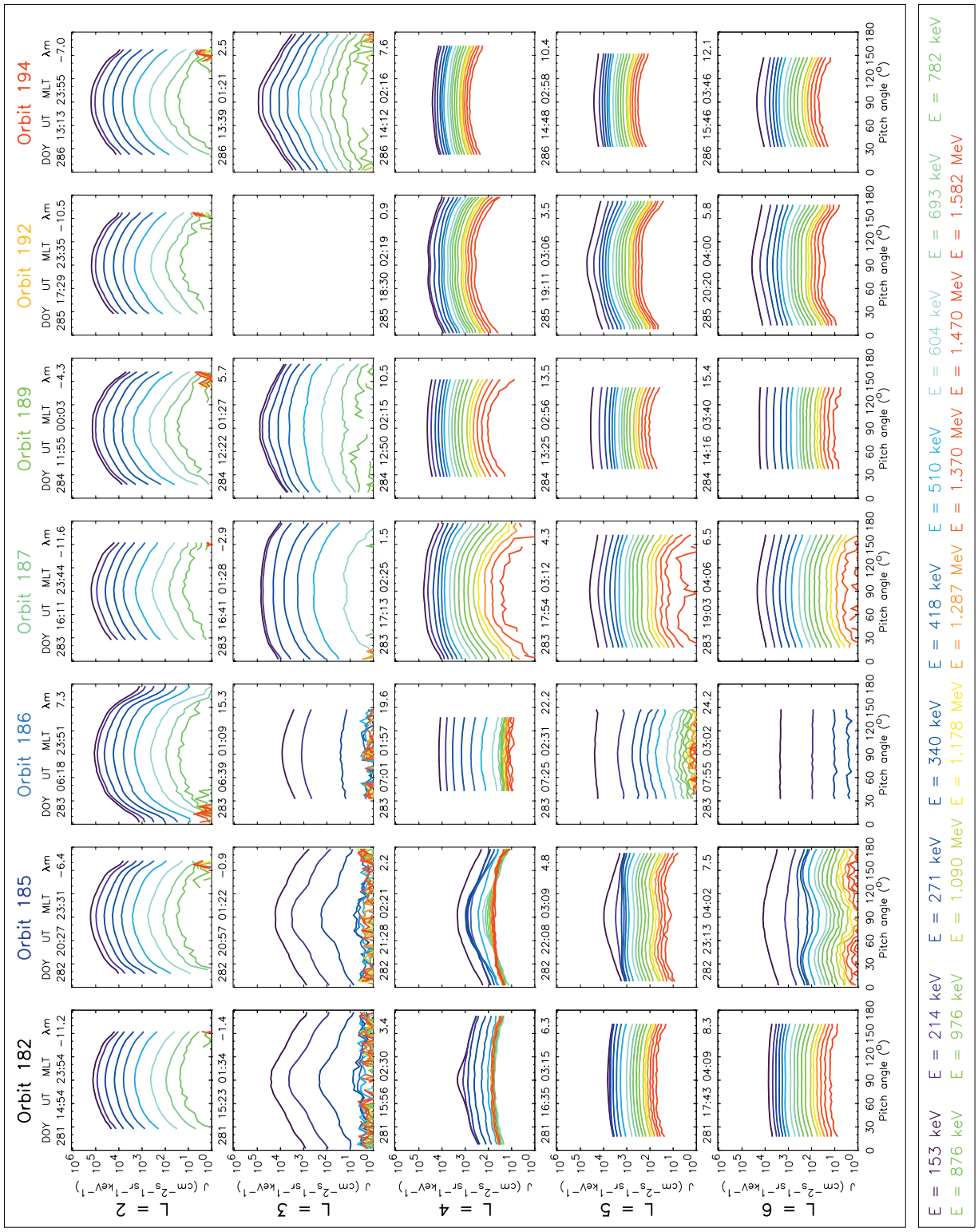
Orbit 182
Orbit 185
Orbit 186
Orbit 187
Orbit 189
Orbit 192
Orbit 194
DOY UT MLT λm
L = 2
L = 3
L = 4
L = 5
L = 6
J (cm⁻²s⁻¹sr⁻¹keV⁻¹)
Pitch angle (°)
E = 153 keV E = 214 keV E = 271 keV E = 340 keV E = 418 keV E = 510 keV E = 604 keV E = 693 keV E = 782 keV
E = 876 keV E = 976 keV E = 1.090 MeV E = 1.178 MeV E = 1.287 MeV E = 1.370 MeV E = 1.470 MeV E = 1.582 MeV

smaller (larger) pitch angles falls rapidly into the loss cone. The small peaks at higher energies and large (small) pitch angles are due to proton contamination in the detector and should be disregarded. Similar types of rounded pitch angle distributions have been observed near $L = 2$ before [e.g., *Lyons and Williams*, 1984] and are typical of that expected as a result of Coulomb collisions. There is remarkably little variation in either the pitch angle distribution or flux levels at $L = 2$ throughout this event. The distributions at this location are not discussed any further.

[25] The prestorm distributions at $L = 3$ correspond to the middle of the quiet time slot region and are characterized by a "pancake" distribution. The pancake is peaked at 90° and is relatively flat between 75° and 105°. The flux drops rapidly between 50° and 75° (105°–130°) and then falls off steadily toward the loss cone. The distribution is present at energies from 153 to 340 keV; higher energies are below the threshold for detection. This type of distribution has been observed before [*West et al.*, 1973] and is a characteristic signature of pitch angle scattering by plasmaspheric hiss [*Lyons et al.*, 1972; *Lyons*, 1974]. The pancake distribution is completely removed during the storm main phase (orbit 186). However, particles with an equatorial pitch angle >60° would not be able to reach the satellite which is at a magnetic latitude (computed for an undistorted field) of $\lambda_m \approx 15°$. Even so, there is no indication of a pancake distribution at the lowest energies on the following orbit (187) where the satellite crossed the equator at $\lambda_m \approx 3°$. At 153 keV, the pitch angle distribution is relatively flat outside the loss cone, but at higher energies (≥604 keV) the distribution is more rounded, and the flux drops rapidly at pitch angles well outside the loss cone. During the recovery phase (orbit 189–194), a pancake distribution begins to reform at the lowest energies shown while the rest of the distribution remains relatively flat, consistent with the typical energy-dependent scattering timescales for resonant interactions with plasmaspheric hiss [*Lyons et al.*, 1972].

[26] At $L = 4$ there is some evidence for a pancake feature at the lowest energies prior to the storm, but otherwise all the higher energies are relatively flat in pitch angle. By orbit 185 peaks in the pitch angle distribution near 90° appear at energies below 700 keV. These peaks are associated with an increase in flux and occurred at the onset of the storm main phase. At higher energies (>1 MeV), the pitch angle distribution remains relatively flat, with no evidence for injection. During the storm main phase (on orbit 186), the pitch angle distributions become isotropic (indicative of strong diffusion scattering) with a flux increase at low energies and a decrease above 700 keV. The pitch angle distributions during the initial recovery phase (orbit 187) have a very different form to the prestorm distributions. Flux increases are observed at all energies, but the increases occur over a wider range of pitch angles at lower energies than at higher energies. The changes in the pitch angle distribution are therefore energy dependent. At high energies, the distribution has a very broad, flat top, but the flux falls very rapidly before the loss cone is reached. At lower energies, the flux does not fall so rapidly toward the loss cone. Since the flux is increasing at this time, and at this location, the pitch angle distribution should be characteristic of the acceleration process. On the following orbits, the flux continues to increase at high energies and the distribution function becomes less anisotropic. A slight minimum at 90° also appears by orbit 192.

[27] The prestorm distributions at $L = 5$ and $L = 6$ are very flat. However, during the magnetopause compression on orbit 185, the distributions near 90° exhibit a peak at low energies and a local minimum for $0.3 \leq E \leq 1.58$ MeV. This type of distribution has been observed before and is referred to as a butterfly distribution [*West et al.*, 1973; *West*, 1979; *Fritz*, 2001; *Selesnick and Blake*, 2002] and sometimes a cigar shaped distribution [*Baker et al.*, 1978]. The butterfly distribution is even more pronounced at $L = 6$, but is no longer present during the main phase (orbit 186). During the recovery phase, the pitch angle distributions at $L = 5$ and $L = 6$ exhibit similar features to those at $L = 4$ and evolve in a similar way. At high energies, the distributions have a broad flat top and fall rapidly toward the loss cone. There is a possible minima near 90°, similar to a butterfly distribution. At lower energies, the flat top becomes narrower and the distribution becomes anisotropic with a peak near 90°.

[28] During the recovery phase the energy spectrum for $3.5 \leq L \leq 6$ becomes harder with time. This can be seen from orbits 187–194 in Figure 3 where the flux at fixed energy become close together, particularly for $L = 4$. This spectral hardening indicates that the acceleration is energy dependent. This is discussed in more detail elsewhere [*Meredith et al.*, 2002b].

5. Discussion

5.1. Butterfly Distributions

[29] Butterfly distributions were observed at the onset of the main phase (orbit 185). They are usually explained in terms of drift shell splitting due to local time asymmetry in the Earth's magnetic field [*Roederer*, 1970]. Figure 2 shows that there is significant structure in the outer radiation belt flux profile on this orbit which also supports the concept of drift shell splitting since a sharp gradient in the radial flux profile should have a larger effect on the flux on different drift shells. Furthermore, magnetopause compression occurred at this time and is also consistent with butterfly distributions due to magnetopause shadowing, i.e., the process whereby 90° particles drift to larger radial distance on the dayside and may be scattered at the magnetopause and hence be lost from the distribution [*West*, 1979; *Selesnick and Blake*, 2002].

[30] There is some evidence for butterfly distributions occurring during the recovery phase where the relativistic electron acceleration is most intense. These distributions occur mainly at high energies for $L \geq 5$, but also for $L \approx 4$ on orbit 192. Theory shows that drift shell splitting should not be energy dependent. One possibility is that the energy

Figure 3. (opposite) Electron pitch angle distributions from the MEA instrument of CRRES for the orbits indicated by the vertical bars in Figure 1. The data are averaged over 0.1 L. The orbits are for prestorm (182), onset of main phase (185), minimum Dst (186), initial recovery (187), and recovery (189–194).

dependence could be due to time of flight effects whereby the higher energy electrons reach the spacecraft before lower energy particles and therefore the signature of magnetopause shadowing should be observable in the higher energy population first. At $L = 4$ the drift period for an equatorially mirroring electron is approximately 12 min at 1.47 MeV and 1.01 hours at 214 keV. Thus the difference in the time of flight is approximately 49 min. At $L = 6$ the drift periods are 8 and 40.3 min at 1.47 MeV and 214 keV, respectively, and thus the difference in the time of flight is approximately 32.3 min. If fact since CRRES is near 0400 MLT the time of flight difference is less than this assuming that magnetopause shadowing occurs near 1200 MLT. Inspection of higher resolution data at $0.1L$ (not shown here) shows that there is a pancake at 214 keV and a butterfly distribution at 1.47 MeV all the way between $L = 5.05–6.05$. Data averaging to achieve a spatial resolution of $0.1L$ takes approximately 3 min at $L = 4$ and 6 min at $L = 6$. However, it takes the spacecraft more than 1 hour to move between these two locations. Thus we conclude that the energy dependence in the butterfly distributions is not due to time of flight effects.

[31] During the recovery phase of this storm *Brautigam and Albert* [2000] demonstrated that lower energy particles are subject to inward radial diffusion while higher energy electrons diffuse outward. The pancake distributions at low energy are consistent with inward radial diffusion, if the anisotropy developed during inward transport is sufficient to overcome drift shell splitting. The small minimum at higher energies is more difficult to explain. Field distortions at $L \approx 4$ should be small, and we would not normally expect significant drift shell splitting. One possibility is that the minimum near 90° is a result of nonlocal acceleration occurring at higher (lower) latitudes. Acceleration near 90° in a localized region along the field line above (below) the equator would result in a distribution with a minimum at 90° when mapped back to the equator.

5.2. Radial Diffusion

[32] A detailed analysis of radial diffusion for the storm event discussed here has been conducted previously by *Brautigam and Albert* [2000], who calculated the change in the electron flux due to both electric and magnetic field fluctuations with an outer boundary at $L = 6.6$. The electron flux at the outer boundary was taken from LANL satellite data, and the diffusion rates were calculated from a time dependent model based on *Kp*. Following the initial flux drop out, the observed recovery phase enhancements agree very well with modeled inward radial diffusion for lower energy electrons with $M = p^2 \sin^2 \alpha/(2\, m_0 B) \leq 314$ MeV/Gauss. However, there were significant discrepancies at higher energies ($M > \sim 700$ MeV/Gauss). First, their model results underestimated the phase space density by a factor of 5 near the inner edge of the outer zone, near $L = 4 - 4.5$. Second, the model could not reproduce the significant increase in flux between $L = 4.0 - 5.5$ in the late recovery period, i.e., between orbits 190–192. Third, during the storm recovery, the observed radial gradient in phase space density became negative, indicative of outward radial diffusion and the existence of a local acceleration source near $L = 4$.

[33] There are features in the pitch angle distributions presented here that are also inconsistent with the concept of pure radial diffusion in which the first two invariants are conserved. Specifically, if radial diffusion is the dominant mechanism responsible for inward radial transport, then we might expect the distributions to become peaked at 90°. Conservation of M implies that the perpendicular momentum $p_\perp$ should increase with $\sqrt{B}$ as the particles diffuse inward. Conservation of the second invariant $J = \int p_{||} ds$ (or integral invariant $I = \int_{s_m}^{s_{m'}} \sqrt{1 - B(s)/B_m} ds$) requires that the parallel momentum $p_{||}$ should scale inversely with the length of the bounce orbit. Particles mirroring at the equator remain at the equator and p should increase with $\sqrt{B}$ as they diffuse in. At other pitch angles the particles diffuse inward on lines of almost constant latitude in a dipole field [*Walt*, 1994, p. 132]. The mirror points converge toward the equator at lower L and so $p_{||}$ increases, but $p_{||}$ does not increase as fast as $p_\perp$. Thus, assuming an isotropic source distribution, the pitch angle distributions should become more anisotropic and peaked near 90°, and the anisotropy should increase with decreasing L. There is some evidence for distributions peaked near 90° at $L = 5 - 6$ at a few hundred keV, but very little evidence at $L = 4$ during the recovery phase. The pancake distributions are consistent with inward radial diffusion at low energies, in agreement with the results of *Brautigam and Albert* [2000], but suggests that another process may be operating near $L = 4$. At MeV energies there is no real evidence for a peak at 90° at $L = 4$ where most of the flux increase takes place. If the source distribution at the outer trapping region is a butterfly distribution then this could result in a flat top distribution after sufficient inward radial diffusion. However, the existing theory of radial diffusion does not explain the energy dependence in the observed pitch angle distributions. In any case, *Brautigam and Albert* [2000] showed that the direction of radial diffusion for these higher energy particles is outward, not inward, and therefore suggests an additional source of acceleration. The fact that energy dependence is observed in the pitch angle distributions is also consistent with more than one source of acceleration.

[34] During the storm main phase, the slot region between the inner and outer zones is filled in at energies of a few hundred keV. The dominant process governing radial transport at these energies is radial diffusion. However, there is no evidence for filling in the slot region at higher energies >500 keV, although the inner edge of the outer boundary moves inward by about $0.3L$. This suggest that either radial diffusion must be energy dependent, or that preferential loss occurs for the high energy population during the main phase of the storm. The latter would require an additional mechanism, which violates the first two adiabatic invariants. The former may also be an indicator as to why radial diffusion cannot account for the increase in flux just outside the slot region near $L \sim 4$. Radial diffusion is most efficient when the frequency of electric and magnetic field fluctuations is comparable to the drift frequency of particles drifting around the Earth. The fact that higher energy particles are not transported into the slot region may be due to insufficient power spectral density over the appropriate frequency range.

5.3. Pitch Angle Scattering by Whistler Mode Waves

[35] During magnetic storms many different types of waves are excited but only five have the possibility of

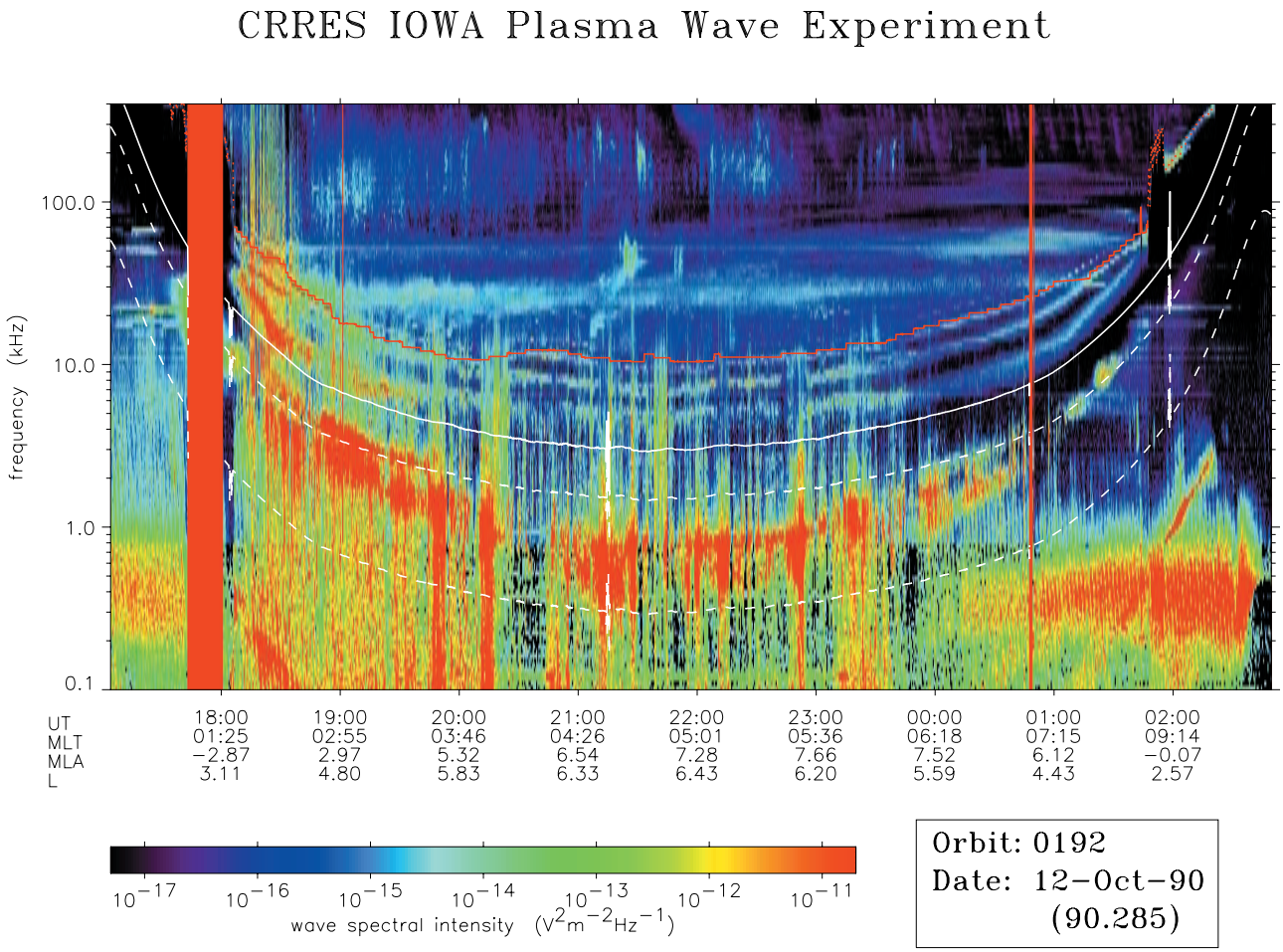

Figure 4. Power spectral density of waves observed by the PWI instrument during the recovery phase of the October 1990 storm (orbit 192). The solid white line indicates the electron gyrofrequency f_{ce}, the dashed lines correspond to 0.5 f_{ce}, and 0.1 f_{ce}, and the long dashed line corresponds to the lower hybrid resonance frequency f_{LHR}. The white dotted lines indicate nf_{ce}. The red line is an estimate of the upper hybrid resonance frequency f_{UHR} calculated from the lower cutoff of electromagnetic continuum radiation and the dashed red line is f_{UHR} calculated from wave emissions at f_{UHR}. The solid red vertical bars indicate data gaps.

resonating with electrons up to MeV energies [*Horne and Thorne*, 1998]. One of the most important types of waves that can energize electrons near $L = 4$ is whistler mode chorus via Doppler shifted cyclotron resonance [*Summers et al.*, 1998; *Summers and Ma*, 2000]. Here we consider whether resonant scattering by these waves can account for the flat top distributions and energy dependence.

[36] Doppler shifted cyclotron resonance between whistler mode waves and electrons depends on the normalized wave frequency f/f_{ce} and the ratio f_{pe}/f_{ce} between the plasma frequency and the electron gyrofrequency. In general whistler mode waves tend to resonate with electrons greater than 10 keV, although it is possible to resonate with much lower energies [*Johnstone et al.*, 1993]. The growth rate of the waves depends on the anisotropy of the distribution and the number of particles in resonance [*Kennel and Petcheck*, 1966]. Since the particle phase space density decreases with increasing energy, wave growth or damping is dominated by the larger flux of lower energy particles in resonance with the waves. Figure 1 shows that the amplitude of whistler mode waves is substantially increased outside the plasmapause after the onset of the storm and during the recovery period. The wave power spectral density is enhanced by several orders of magnitude above prestorm levels in the region near $L = 4$ where most of the acceleration is observed to take place. The increased whistler mode wave power is directly related to enhancements in the flux of 14.3 keV (and to a lesser extent 214 keV) electrons, which are injected into the outer radiation zone during substorm activity (enhanced AE) during both the main phase and recovery of the storm.

[37] An example wave spectrogram of the power spectral density of waves observed during the recovery phase is shown in Figure 4 (orbit 192). The electron gyrofrequency is shown as a solid white line, the dashed white lines below f_{ce} correspond to 0.5 f_{ce}, 0.1 f_{ce} and the lower hybrid resonance frequency f_{LHR}, while the dotted white lines above f_{ce} correspond to harmonics nf_{ce}. The solid red line indicates the upper hybrid resonance frequency $f_{UHR} = (f_{pe}^2 + f_{ce}^2)^{1/2}$ calculated from the lower frequency cut-off of electromag-

netic continuum radiation and the red dashed line is f_{UHR} calculated from wave emissions at f_{UHR} inside the plasmasphere. Typically, $2 < f_{pe}/f_{ce} < 5$ during the event [*Meredith et al.*, 2002b]. Strong whistler mode chorus waves between 0.5 and 0.1 f_{ce} are detected once the spacecraft leaves the high density plasmapause region and are present for most of the orbit until the spacecraft reenters the plasmapause just before 0200 UT. Note that the chorus amplitudes can be bursty and the frequency can extend below 0.1 f_{ce}. The band of emissions that occur below 0.1 f_{ce} after 0000 UT and which do not scale with the gyrofrequency are an example of plasmaspheric hiss that has escaped from the plasmapause region. Both chorus and hiss can contribute to pitch angle scattering [*Lyons et al.*, 1972].

[38] Anisotropic electrons in the energy range (10–100 keV) are required to drive whistler mode waves unstable. Wave growth is associated with a net transfer of energy from the particles to the waves as resonant electrons diffuse toward the loss cone [*Kennel and Petschek*, 1966]. The energization of the high energy electrons requires reabsorption of the wave energy. However, for a sufficiently anisotropic distribution, the contribution to wave growth from scattering at low energies where the flux is generally higher may overcome the contribution to wave damping at high energies where the flux is much lower. Under these conditions, it is possible to have particle energization and wave growth, provided resonance extends over a sufficiently large range of energies.

[39] Wave growth usually results in scattering into the loss cone, and hence precipitation [*Gendrin*, 1981]. Wave damping is usually associated with scattering to larger pitch angles and particle trapping [e.g., *Thorne and Horne*, 1996]. The two processes act over different range of pitch angles, and energies, although in some cases the regions may overlap. This raises the question as to whether the whistler mode waves observed during the storm resonate with the particles over a sufficiently large range of pitch angles and energies so as to be able to scatter them to higher energies, without being lost. To consider this in more detail, we have constructed the following model. We consider parallel propagating whistler mode waves only. These waves have the largest growth rates and should dominate the wave spectrum. Furthermore, the dominant contribution to scattering is from the first order cyclotron resonance. Higher order scattering by oblique waves is a second order effect [*Lyons et al.*, 1971]. We consider waves traveling in both directions along the magnetic field. We assume a value for f_{pe}/f_{ce} and a frequency bandwidth characteristic of the upper and lower frequencies f_1/f_{ce} and f_2/f_{ce} of observed chorus emissions. We then compute the pitch angles corresponding to the intersection of a curve of constant energy with the resonant ellipse for each whistler mode wave. The ellipse is obtained from the resonance condition

$$v_{\parallel} = \frac{\omega}{k_{\parallel}}\left(1 - \frac{n\Omega_{\sigma}}{\omega\gamma}\right) \tag{2}$$

which can be rewritten in the form of an ellipse

$$\frac{v_{\perp}^2}{a^2} + \frac{\left(v_{\parallel} - d\right)^2}{b^2} = 1 \tag{3}$$

where

$$a^2 = c^2\left[1 - \frac{(\omega/\Omega_{\sigma})^2}{(n^2 + h^2)}\right] \tag{4}$$

$$b^2 = \frac{n^2 a^2}{(n^2 + h^2)} \tag{5}$$

$$h = \mu_{\parallel}\frac{\omega}{\Omega_{\sigma}} \tag{6}$$

and

$$d = \frac{\omega}{\Omega_{\sigma}}\frac{ch}{(n^2 + h^2)} \tag{7}$$

where $\mu_{\parallel}$ is the refractive index for parallel propagating whistler mode waves and c is the speed of light. The calculations are only shown for the $n = -1$ resonance (where $\Omega_{\sigma} = -|\Omega_e|$ for electrons), which is the only one allowed for propagation parallel to $\mathbf{B_0}$.

[40] The outer zone electrons execute many drift periods during the period of observation, and the ratios f_{pe}/f_{ce}, f_1/f_{ce}, and f_2/f_{ce} may vary significantly during a drift orbit. In the low density region outside the plasmapause, it is difficult to calculate the ratio f_{pe}/f_{ce} from the wave spectra. Electrostatic electron cyclotron harmonic wave emissions at $(n + \frac{1}{2})f_{ce}$ can dominate the wave spectrum up to and above the local upper hybrid frequency (see Figure 4, just after 1800 UT). Estimates of f_{pe} from the lower frequency cut-off of electromagnetic continuum radiation may give an overestimate as density irregularities may scatter and reflect continuum radiation preventing the lower frequency component from reaching the spacecraft. We have therefore selected $f_{pe}/f_{ce} = 5$ and 1 as being representative of the range of values outside the plasmapause during storm times. For a representative chorus bandwidth we adopt an upper cutoff $f_1/f_{ce} = 0.75$ and a lower cutoff f_2/f_{ce} between 0.05 and 0.2. The results are shown in Figure 5.

[41] For $f_{pe}/f_{ce} = 5$ the range of pitch angles resonant with the waves is very small at energies >200 keV (Figures 5a and 5b). At 14 keV the range is much wider and extends into the loss cone. Reducing the lower frequency limit f_2/f_{ce} from 0.2 to 0.05 (Figure 5b) increases the range of resonant pitch angles, mainly at energies of a few hundred keV. However, the range of pitch angles at ~MeV is still very small, much smaller than the observed range of flat pitch angles at $L = 4$, orbits 187–192, shown in Figure 3. Reducing the ratio f_{pe}/f_{ce} to 1 substantially increases the range of resonant pitch angles (Figure 5c), particularly at a few hundred keV. Particles can be scattered into the loss cone for $E <\sim 200$ keV, contributing to wave growth, but at higher energies they are trapped and can undergo acceleration over a range of pitch angles near 90° as waves are absorbed. However, the range of resonant pitch angles at $E > \sim 0.5$ MeV is still too small to account for observations. Reducing the lower frequency limit from 0.2 to 0.05 in the low density case (Figure 5d) increases the range or resonant pitch angles further, comparable to the width of the observed flat top distribution at 1.5 MeV during the recovery phase.

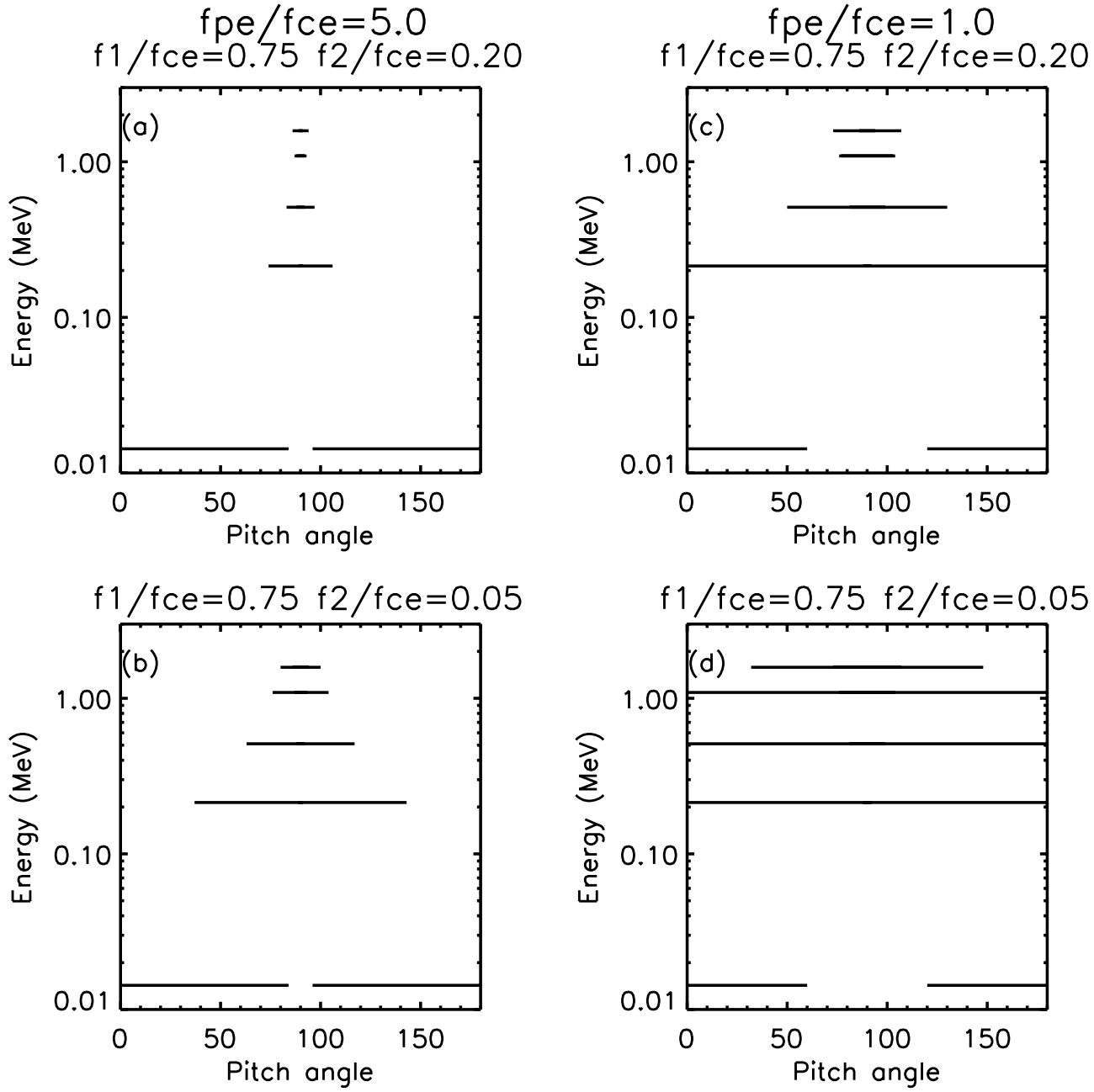

Figure 5. Range of pitch angles resonant with a band of parallel propagating whistler mode waves at energies of 14.3 214, 512, 1.09 $\times$ 10^3 and 1.53 $\times$ 10^3 keV. The upper and lower frequency band is denoted by f_1/f_{ce} and f_2/f_{ce}, respectively.

[42] It is not possible to match the shape of the pitch angle distribution function in more detail since this depends on the pitch angle and energy diffusion coefficients, and one must also take into account the angular distribution of the waves and the resonant wave power at all cyclotron resonant harmonics along the field line. However, since parallel propagating waves should dominate the spectrum locally, they should provide a reasonable first approximation. The results in Figure 5 exhibit one of the general features of the observed pitch angle distributions; the range of resonant pitch angles is strongly energy dependent, and increases in width with decreasing energy.

[43] For pitch angles $\alpha \neq 90°$ energization can only occur as the particles are scattered in pitch angle [*Gendrin*, 1981; *Summers and Ma*, 2000; *Summers et al.*, 1998]. As the particles execute many drift orbits during the acceleration, and encounter a range of different plasma densities and frequency bandwidths, they can be scattered in pitch angle and energy many times. The distribution function may therefore become enhanced but relatively flat over the range of pitch angles shown (Figure 5), provided the particles encounter regions of sufficiently low plasma density where $f_{pe}/f_{ce} \sim 1$.

[44] We conclude that the flat top distributions are consistent with wave particle interactions. Furthermore, since

the flat top distributions observed during the storm recovery phase exhibit strong gradients into the loss cone at high energies, scattering into the loss cone is very weak at best. This is also consistent with the fact that the range of resonant pitch angles does not extend into the loss cone at high energies (>500 keV).

[45] The results in Figure 5 also predict that at energies of ~14 keV, there is little or no scattering near 90°. It may be possible for the waves to form pancake distributions at these energies as particles at smaller pitch angles are scattered into the loss cone, leaving behind the trapped remnant of the distribution. Such pancakes have been observed to form on a timescale of approximately 4 hours after a substorm injection [*Meredith et al.*, 2000]. The calculations here suggest that pancakes may form at ~10 keV during the recovery phase of a magnetic storm while particles at higher energies are accelerated to MeV energies.

6. Summary and Conclusions

[46] We have examined the pitch angle distributions of 0.15–1.58 MeV electrons during the October 1990 storm event observed by the CRRES spacecraft. The pitch angle distributions were obtained over a period of 5 days during outbound orbits of the spacecraft within the region 2354–0400 MLT. During this storm, the highest increase in electron flux occurred near the inner edge of the outer radiation belt, near $L = 4$. At this location, flux levels during the recovery phase rose to more than an order of magnitude greater than the prestorm level at energies of ~1 MeV. In comparison to $L = 4$, very little overall variation in the MeV flux was observed near geostationary orbit.

[47] Rounded pitch angle distributions are observed at the outer edge of the inner zone at $L \approx 2$. They show very little change during the storm event. The rounded shape suggests they are characteristic of collision-dominated distributions.

[48] Pancake distributions are observed in the slot region at $L \approx 3$ before the storm. The pancakes are removed during the main phase and re-form during the late recovery phase. These distributions are characteristic of pitch angle scattering into the loss cone by plasmaspheric hiss.

[49] At $L \approx 4$, the distributions exhibit a weak pancake at low energies before the storm main phase. During the recovery phase, the distributions are observed to be energy dependent. They exhibit a flat top distribution at energies 0.153–1.58 MeV over a broad range of pitch angles. Flat top distributions are broader at lower energies (30°–150°) than higher energies (50°–130°). The higher energies exhibit a much faster fall off toward the loss cone than at lower energies. Broad flat top distributions appear at the time and region of highest electron flux enhancements.

[50] In the outer radiation zone ($L = 5 - 6$), the pitch angle distributions are flat before the storm. At storm onset butterfly distributions are initially observed, prior to the flux drop out during the main phase. During the recovery phase, flat top distributions are observed at high energies (> ~500 keV). During the late recovery, there is evidence for a weak pancake distributions at low energies of a few hundred keV and butterfly distributions at higher energies.

[51] We conclude that flat top distributions at MeV energies are characteristic of electron acceleration near the inner edge of the outer zone during the recovery phase. Although radial diffusion may be an important factor contributing to the enhanced electron flux, the existing theory does not seem to account for the energy dependence of the observed pitch angle distributions adequately, suggesting an additional acceleration source. The distributions are consistent with pitch angle scattering by Doppler shifted cyclotron resonance with whistler mode waves under certain constraints. Calculations of the pitch angles resonant with whistler mode waves requires the interactions to take place in regions of relatively low plasma density ($f_{pe}/f_{ce} \approx 1$) in order to obtain flat top distributions. This is also one of the conditions for efficient energization of the particles by the waves [*Summers et al.*, 1998]. The region of acceleration should be confined to the low density region outside the plasmapause, the region where intense whistler mode chorus waves are observed.

[52] **Acknowledgments.** We thank A. L. Vampola for supplying the CRRES/MEAdata and for his assistance in their analysis and interpretation. We thank the World Data Center C1 for STP at the Rutherford Appleton Laboratory and the NSSDC Omniweb for providing the geomagnetic indices and solar wind parameters used in this paper. This work is supported by the UK Natural Environment Research Council and NASA grant NAG5-11922.

References

Anderson, R. R., D. A. Gurnett, and D. L. Odem, CRRES plasma wave experiment, *J. Spacecr. Rockets*, *29*, 570, 1992.

Baker, D. N., P. R. Higbie, and E. W. Hones Jr., High resolution energetic particle measurements at 6.6 Re, 3, Low energy electron anisotropies and short term substorm predictions, *J. Geophys. Res.*, *83*, 4863, 1978.

Baker, D. N., J. B. Blake, L. B. Callis, R. D. Belian, and T. E. Cayton, Relativistic electrons near geostationary orbit: Evidence for internal magnetospheric acceleration, *Geophys. Res. Lett.*, *16*, 559, 1989.

Baker, D. N., et al., Recurrent geomagnetic storms and relativistic electron enhancements in the outer magnetosphere: ISTP coordinated measurements, *J. Geophys. Res.*, *102*, 14,141, 1997.

Baker, D. N., et al., A strong CME-related magnetic cloud interaction with the Earth's magnetosphere: ISTP observations of rapid relativistic electron acceleration on May 15, 1997, *Geophys. Res. Lett.*, *25*, 2975–2978, 1998a.

Baker, D. N., T. I. Pulkkinen, X. Li, S. G. Kanekal, J. B. Blake, R. S. Selesnick, M. G. Henderson, G. D. Reeves, H. E. Spence, and G. Rostoker, Coronal mass ejections, magnetic clouds, and relativistic magnetospheric electron events: ISTP, *J. Geophys. Res.*, *103*, 17,279–17,291, 1998b.

Blake, J. B., D. N. Baker, N. Turner, K. W. Olgilvie, and R. P. Lepping, Correlation of changes in the outer-zone relativistic-electron population with upstream solar wind and magnetic field measurements, *Geophys. Res. Lett.*, *24*, 927, 1997.

Brautigam, D. H., and J. M. Albert, Radial diffusion analysis of outer radiation belt electrons during the 9 October 1990, magnetic storm, *J. Geophys. Res.*, *105*, 291, 2000.

Buhler, P. A. Johnstone, L. Desorgher, A. Zehnder, E. Daly, and L. Adams, The outer radiation belt during the CME event, 10 January, 1997, *Geophys. Res. Lett.*, *25*, 2983–2986, 1997.

Carpenter, D. L., and R. R. Anderson, An ISEE/Whistler model of equatorial electron density in the magnetosphere, *J. Geophys. Res.*, *97*, 1097, 1992.

Elkington, S. R., M. K. Hudson, and A. A. Chan, Acceleration of relativistic electrons via drift resonant interactions with toroidal-mode Pc-5 ULF oscillations, *Geophys. Res. Lett.*, *26*, 3273, 1999.

Friedel, R. H. W., G. D. Reeves, and T. Obara, Relativistic electron dynamics in the inner magnetosphere—A review, *J. Atmos. Sol. Terr. Phys.*, *64*, 265, 2002.

Fritz, T., The cusp as a source of magnetospheric energetic particles, currents, and electric fields: A new paradigm, *Space Sci. Rev.*, *95*, 469, 2001.

Fujimoto, M., and A. Nishida, Energization and anisotropization of energetic electrons in the Earth's radiation belt by the recirculation process, *J. Geophys. Res.*, *95*, 4265, 1990.

Gendrin, R., General relationships between wave amplification and particle diffusion in a magnetoplasma, *Rev. Geophys. Space Phys.*, *19*, 171, 1981.

Hardy, D. A., D. M. Walton, A. D. Johnstone, M. F. Smith, M. P. Gough, A. Huber, J. Pantazis, and R. Burkhardt, The low energy plasma analyser, *IEEE Trans. Nucl. Sci.*, *40*(2), 246, 1993.

Horne, R. B., The contribution of wave particle interactions to electron loss and acceleration in the Earth's radiation belts during geomagnetic storms, in *Review of Radio Science 1999–2002*, edited by W. R. Stone, pp. 801–828, John Wiley, New York, 2002.

Horne, R. B., and R. M. Thorne, Potential waves for relativistic electron scattering and stochastic acceleration during magnetic storms, *Geophys. Res. Lett.*, *25*, 3011, 1998.

Hudson, M. K., S. R. Elkington, J. G. Lyon, and C. C. Goodrich, Increase in relativistic electron flux in the inner magnetosphere: ULF wave mode structure, *Adv. Space Res.*, *25*, 2327, 2000.

Iles, R. H. A., A. N. Fazakerley, A. D. Johnstone, N. P. Meredith, and P. Buhler, The relativistic electron response in the outer radiation belt during magnetic storms, *Ann. Geophys.*, *20*, 957–965, 2002.

Johnstone, A. D., D. M. Walton, R. Liu, and D. Hardy, Pitch angle diffusion of low-energy electrons by whistler mode waves, *J. Geophys. Res.*, *98*, 5959, 1993.

Johnstone, A. D., D. J. Rodgers, and G. H. Jones, Statistical studies of energetic electrons in the outer radiation belt, in *Radiation Measurements*, vol. 30, p. 625, Elsevier Sci., 1999.

Kennel, C. F., and H. E. Petschek, Limit on stably trapped particle fluxes, *J. Geophys. Res.*, *71*, 1, 1966.

Li, X., and M. A. Temerin, The electron radiation belt, *Space Sci. Rev.*, *95*, 569, 2001.

Li, X., D. N. Baker, M. Temerin, T. E. Cayton, G. D. Reeves, R. A. Christiansen, J. B. Blake, M. D. Looper, R. Nakamura, and S. G. Kanekal, Multi-satellite observations of the outer zone electron variation during the November 3–4, 1993, magnetic storm, *J. Geophys. Res.*, *102*, 14,123, 1997a.

Li, X., D. N. Baker, M. Temerin, D. Larson, R. P. Lin, G. D. Reeves, M. Looper, S. G. Kanekal, and R. A. Mewaldt, Are energetic electrons in the solar wind the source of the outer radiation belt?, *Geophys. Res. Lett.*, *24*, 923, 1997b.

Li, X., D. N. Baker, M. Temerin, T. E. Cayton, E. G. D. Reeves, T. Araki, H. Singer, D. Larson, R. P. Lin, and S. G. Kanekal, Energetic electron injections into the inner magnetosphere during the January 10–11 1997 magnetic cloud event, *Geophys. Res. Lett.*, *25*, 2561–2564, 1998.

Liu, W. W., G. Rostoker, and D. N. Baker, Internal acceleration of relativistic electrons by large amplitude ULF pulsations, *J. Geophys. Res.*, *104*, 17,391, 1999.

Loewe, C. A., and G. W. Prölss, Classification and mean behaviour of magnetic storms, *J. Geophys. Res.*, *102*, 14,209, 1997.

Lyons, L. R., Pitch angle and energy diffusion coefficients from resonant interactions with ion-cyclotron and whistler waves, *J. Plasma Phys.*, *12*, 417, 1974.

Lyons, L. R., and D. A. Williams, *Quantitative Aspects of Magnetospheric Physics*, D. Reidel, Norwell, Mass., 1984.

Lyons, L. R., R. M. Thorne, and C. F. Kennel, Electron pitch-angle diffusion driven by oblique whistler-mode turbulence, *J. Plasma Phys.*, *6*, 589, 1971.

Lyons, L. R., R. M. Thorne, and C. F. Kennel, Pitch-angle diffusion of radiation belt electrons within the plasmasphere, *J. Geophys. Res.*, *77*, 3455, 1972.

Meredith, N. P., R. B. Horne, A. D. Johnstone, and R. R. Anderson, The temporal evolution of electron distributions and associated wave activity following substorm injections in the inner magnetosphere, *J. Geophys. Res.*, *105*, 12,907, 2000.

Meredith, N. P., R. B. Horne, and R. R. Anderson, Substorm dependence of chorus amplitudes: Implications for the acceleration of electrons to relativistic energies, *J. Geophys. Res.*, *106*, 13,165, 2001.

Meredith, N. P., R. B. Horne, R. H. A. Iles, R. M. Thorne, D. Heynderickx, and R. R. Anderson, Outer zone relativistic electron acceleration associated with substorm enhanced whistler mode chorus, *J. Geophys. Res.*, *107*(A7), 1144, doi:10.1029/2001JA900146, 2002a.

Meredith, N. P., R. B. Horne, D. Summers, R. M. Thorne, R. H. A. Iles, D. Heynderickx, and R. R. Anderson, Evidence for acceleration of outer zone electrons to relativistic energies by whistler mode chorus, *Ann. Geophys.*, *20*, 967–974, 2002b.

Miyoshi, Y., A. Morioka, T. Obara, H. Misawa, T. Nagai, and Y. Kasahara, Rebuilding process of the outer radiation belt during the November 3, 1993, magnetic storm: NOAA and EXOS-D observation, *J. Geophys. Res.*, *107*, in press, 2002.

Reeves, G. D., Observations of relativistic electron coherence as a function of energy, L-shell, and pitch angle, paper presented at Int. Space Environ. Cont., Rice Space Inst., Rice Univ., Queenstown, N.Z., 23–27 July 2001.

Reeves, G. D., Relativistic electrons and magnetic storms: 1992–1995, *Geophys. Res. Lett.*, *25*, 1817, 1998.

Reeves, G. D., D. N. Baker, R. D. Belian, J. B. Blake, T. E. Cayton, J. F. Fennel, R. H. W. Friedel, M. M. Meier, R. S. Selesnick, and H. E. Spence, The global response of relativistic electrons to the January 1997 magnetic cloud, *Geophys. Res. Lett.*, *25*, 3265–3268, 1998a.

Reeves, G. D., R. H. W. Friedel, R. D. Belian, M. M. Meier, M. G. Henderson, T. Onsager, H. J. Singer, D. N. Baker, X. Li, and J. B. Blake, The relativistic electron response at geosynchronous orbit during the January 1997 magnetic storm, *J. Geophys. Res.*, *103*, 17,559–17,570, 1998b.

Roderer, J. G., *Dynamics of Geomagnetically Trapped Radiation*, Springer-Verlag, New York, 1970.

Rostoker, G., S. Skone, and D. N. Baker, On the origin of relativistic electrons in the magnetosphere associated with some geomagnetic storms, *Geophys. Res. Lett.*, *25*, 3701, 1998.

Schulz, M., and L. Lanzerotti, *Particle Diffusion in the Radiation Belts*, Springer-Verlag, New York, 1974.

Selesnick, R. S., and J. B. Blake, Radiation belt electron observations following the January 1997 magnetic cloud event, *Geophys. Res. Lett.*, *25*, 2553–2556, 1998.

Selesnick, R. S., and J. B. Blake, Relativistic electron drift shell splitting, *J. Geophys. Res.*, *107*(A9), 1265, doi:10.1029/2001JA009179, 2002.

Singer, H. J., W. P. Sullivan, P. Anderson, F. Mozer, P. Harvey, J. Wygant, and W. McNeil, Fluxgate magnetometer instrument on the CRRES, *J. Spacecr. Rockets*, *29*, 599, 1992.

Summers, D., and C. Ma, A model for generating relativistic electrons in the Earth's inner magnetosphere based on gyroresonant wave-particle interactions, *J. Geophys. Res.*, *105*, 2625, 2000.

Summers, D., R. M. Thorne, and F. Xiaio, Relativistic theory of wave-particle resonant diffusion with application to electron acceleration in the magnetosphere, *J. Geophys. Res.*, *103*, 487, 1998.

Thorne, R. M., and R. B. Horne, Whistler absorption and electron heating near the plasmapause, *J. Geophys. Res.*, *101*, 4917, 1996.

Thorne, R. M., and C. F. Kennel, Relativistic electron precipitation during magnetic storm main phase, *J. Geophys. Res.*, *76*, 4446, 1971.

Vampola, A. L., J. V. Osborn, and B. M. Johnson, CRRES magnetic electron spectrometer, *J. Spacecr. Rockets*, *29*, 592, 1992.

Walt, M., *Introduction to Geomagnetically Trapped Radiation*, Cambridge Univ. Press., New York, 1994.

West, H. I., Jr., R. M. Buck, and R. J. Walton, Electron pitch angle distributions throughout the magnetosphere as observed by OGO 5, *J. Geophys. Res.*, *78*, 1064, 1973.

West, H. I., The signatures of the various regions of the outer magnetosphere in the pitch angle distributions of energetic particles, in *Quantitative Modelling of Magnetospheric Processes*, *Geophys. Monogr. Ser.*, vol. 21, edited by W. P. Olsen, pp. 150–179, AGU, Washington, D. C., 1979.

Wrenn, G. L., and R. J. K. Smith, The ESD threat to GEO satellites: Empirical models for observed effects due to both surface and internal charging, in *ESA Symposium Proceedings on 'Environment Modelling for Space-Based Applications'*, *SP-392*, ESTEC, Noorwijk, Netherlands, p. 121, 1996.

R. R. Anderson, Department of Physics and Astronomy, University of Iowa, Iowa City, IA 52242-1479, USA. (anderson@iowave.physics.uiowa.edu)

D. Heynderickx, Belgian Institute for Space Aeronomy, Ringlaan 3, Brussels, Belgium. (D.Heynderickx.oma.be)

R. B. Horne, British Antarctic Survey, Natural Environment Research Council, Madingley Road, Cambridge CB3 0ET, UK. (r.horne@bas.ac.uk)

R. H. A. Iles and N. P. Meredith Mullard Space Science Laboratory, University College London, Holmbury St. Mary, Dorking, Surrey RH5 6NT, UK. (rhi@mssl.ucl.ac.uk; npm@mssl.ucl.ac.uk)

R. M. Thorne, Department of Atmospheric Sciences, University of California, Los Angeles, 405 Hilgard Avenue, Los Angeles, CA 90095, UK. (rmt@atmos.ucla.edu)